TECHNICAL ARTICLE

Domain structure of CoIr nanoalloys

Evgeny Yu. Filatov,[1,2,a)] Svetlana V. Cherepanova,[1,3] Ilia V. Kochetygov,[1,2] Yury V. Shubin,[1,2] and Sergey V. Korenev[1,2]
[1]*Novosibirsk State University, Pirogova str. 2, 630090 Novosibirsk, Russian Federation*
[2]*Nikolaev Institute of Inorganic Chemistry SB RAS, Lavrentyev Ave. 3, 630090 Novosibirsk, Russian Federation*
[3]*Boreskov Institute of Catalysis SB RAS, Lavrentieva Ave. 5, 630090 Novosibirsk, Russian Federation*

(Received 15 October 2016; accepted 2 March 2017)

X-ray diffraction (XRD) pattern of nanosized equimolar solid solution CoIr prepared by thermolysis of $[Co(NH_3)_6][Ir(C_2O_4)_3]$ contains peaks characteristic of both face-centered cubic (fcc) and hexagonal close-packed (hcp) structure. Moreover, *101* peak of hcp modification is substantially wider than *100* and *002* peaks, *102* and *103* are very broad and almost invisible. Peak *200* of fcc structure is wider than the other peaks of this modification and slightly shifted toward lower angles. It was shown by simulation of XRD patterns that particles of CoIr alloy are nanoheterogeneous and consist of lamellar domains having fcc and hcp structures. The best fit was obtained for the following model parameters: an average crystallites size is about 10 nm, average thicknesses of the fcc and hcp domains are 1.7 and 1.1 respectively. The presence of domain structure was confirmed by transmission electron microscopy data. © *2017 International Centre for Diffraction Data*. [doi:10.1017/S0885715617000367]

Key words: domain structure, powder diffraction, nanoparticles, cobalt, iridium

I. INTRODUCTION

In spite of the small stocks in the Earth's crust, iridium is attractive for use in applications such as biology (Liu and Sadler, 2014; Zhong *et al*., 2015) and catalysis (Firdous *et al*., 2015; Slavcheva *et al*., 2015; Tetlow *et al*., 2016). The general approach which is used to lower the cost of the final product is a reduction of the content of the active phase in the sample because of an increase of specific surface and dilution with the cheaper metal, i.e. obtain solid solutions of metals (Potemkin *et al*., 2012; Firdous *et al*., 2015). Mentioned approach can be implemented by yielding nanoscale solid solutions (nanoalloys) by thermolysis of the single-source precursors such as a double-complex salts (DCS) (Martynova *et al*., 2014; Asanova *et al*., 2016). The salts with oxalate anions are particularly advantageous as they have pronounced reductive properties. Synthesis of DCS simultaneously containing a first raw transition metal and a platinum family metal combined with oxalate as the ligand is appealing, for these compounds can serve as precursors of corresponding nanocrystalline alloys. Such materials can be used for development of novel catalytic systems having a reduced content of noble metals (Potemkin *et al*., 2014; Vedyagin *et al*., 2014; Plyusnin *et al*., 2015).

In our previous work, the structure and thermal decomposition of the $[Co(NH_3)_6][Ir(C_2O_4)_3]$ compound have been studied in helium and hydrogen atmospheres (Filatov *et al*., 2009). The point of this paper is an examination and correct description of the disordered structure of final product of this DCS thermolysis—equimolar nanoalloy CoIr with domain structure.

a)Author to whom correspondence should be addressed. Electronic mail: decan@niic.nsc.ru

II. EXPERIMENTAL

A. Preparation of the precursor and nanoalloys

The synthesis of the precursor was denoted in the work (Filatov *et al*., 2009). To synthesize bimetallic powders in a hydrogen atmosphere, weighted samples of the DCS (~50 mg) were placed in a quartz boat and put in a tubular quartz reactor. Heating was performed in a split furnace at the rate of 20 °C min^{-1}. The temperature was measured with a thermocouple embedded in the oven and adjusted by Omron temperature controller. Additional external thermocouple was used to monitor the correspondence of the sample temperature in the furnace and a specified temperature.

After reaching the final temperature (500 °C in this work), the samples were tempered for 1 h, and then the hydrogen stream was switched off and the system was purged with helium for 30 min. Afterward, the heater was removed and the reactor was allowed to cool to ambient temperature in a continuous helium stream.

B. Instrumentation

Powder X-ray diffraction (XRD) studies of thermolysis products of the prepared compound were made over the 2θ range 5°–120° (step 0.03, collecting time is 3 s) on a DRON-RM4 diffractometer (Cu$K\alpha$-radiation, graphite monochromator on the diffracted beam, ambient temperature). The refinement of lattice parameters was performed by the full profile technique applied to full-range diffraction data using PowderCell 2.4 program (Kraus and Nolze, 2000). The crystallite sizes of the metal phases were determined by the Scherrer equation [WINFIT 1.2.1 (Krumm, 1995)]. High-resolution transmission electron microscopy (HRTEM) measurements were performed using a JEM-2010 electron microscope (lattice plane resolution 0.14 nm at an accelerating

voltage of 200 kV). Images of periodic structures were analyzed by Fourier method. Local energy-dispersive X-ray analysis (EDXA) was carried out using an EDX spectrometer (EDAX Co.) fitted with a Si (Li) detector with a resolution of 130 eV. The error of the metal particle composition determination typically was not <0.05 at.%. The samples for the HRTEM study were prepared on perforated carbon film mounted on a copper grid.

III. RESULTS AND DISCUSSION

The transition temperature $Co_{hcp} \rightarrow Co_{fcc}$ is equal to 420 °C. The iridium (Ir) has face-centered cubic (fcc) structure in all temperature range from room up to melting one. Thus, Köster and Horn said that cobalt (Co) and Ir form a continuous solid solution in the fcc phase and the homogeneous hexagonal close-packed (hcp) solid solution extends to ~63 at.% Ir at 500 °C (Köster and Horn, 1952).

Relatively fast (0.5 h) heating of the sample of the complex $[Co(NH_3)_6][Ir(C_2O_4)_3]$ to 500 °C and further exposure of thermolysis product to this temperature for 1 h results in the formation of CoIr alloy with an unusual XRD pattern. The observed diffraction pattern (see Figure 1) could be interpreted as a pattern of the two-phase system because peaks of fcc and hcp modifications of Co–Ir solid solution are observed. However, it can be seen that *101* peak of hcp modification is substantially wider than *100* and *002* peaks, *102* and *103* are very broad and almost invisible (see Table I). Peak *200* of fcc structure is wider than the other peaks of this modification and slightly shifted toward lower angles. It has been suggested that the particles of the sample have the domain structure where domains of fcc structure alternate with domains of hcp structure as it was in the particles of pure Co (Tsybulya *et al.*, 1999; Cherepanova and Tsybulya, 2004; Cherepanova, 2012).

To test this assumption an appropriate simulations of diffraction patterns using respective software have been done (Cherepanova and Tsybulya, 2004). The calculations are carried out on the basis of the model of one-dimensionally (1D) disordered crystal. The model represents a statistical sequence of the two-dimensionally periodic layers.

The domain structure of Co–Ir alloy was built with Co–Ir layers in hexagonal metric as in hcp structure. Unit-cell parameters determining the layer structure were calculated from the refined unit-cell parameter of fcc structure $a_{cub} = 3.6843$ Å using the formulas $a = b = a_{cub}/\sqrt{2} = 2.605$ and $c = 2a_{cub}/\sqrt{3} = 4.254$ Å. The c unit-cell parameter determines the thickness of two close-packed layers AB. This two-layered fragment is convenient to choose as one layer in the model. Unit cell contains two atoms in positions $M1(0, 0, 0)$ and $M2(2/3, 1/3, 1/2)$, which are statistically occupied by Co and Ir atoms (Co:Ir = 1). Structure of cubic modification AB–CA–BC… can be constructed by sequential tangential displacement of the AB layer on the vector (1/3, 2/3). Structure of hexagonal modification AB–AB… can be simulated by superposition of AB layer on itself without tangential shifts. Thereby both modifications can be simulated by setting the structure of AB layer and two different ways of superposition of the AB layer on itself. Tangential displacements of the AB layer on the vectors (1/3, 2/3) and (0, 0) were marked as first and second ways of superposition of adjacent AB layers. Average thicknesses of domains having fcc and hcp structures were varied by two statistical parameters: *the probability of occurrence of the second superposition way* W_2 and *the conditional probability of repetition of the second superposition way after second superposition way* P_{22}.

Let us consider sense of statistical parameters. W_1 and W_2 are the probabilities of appearance of two-layered fragments of fcc structure (AB–CA or CA–BC or BC–AB) and hcp structure (AB–AB or CA–CA or BC–BC). Parameters $W_{11} = W_1 \bullet P_{11}$ and $W_{22} = W_2 \bullet P_{22}$ are the probabilities of existence

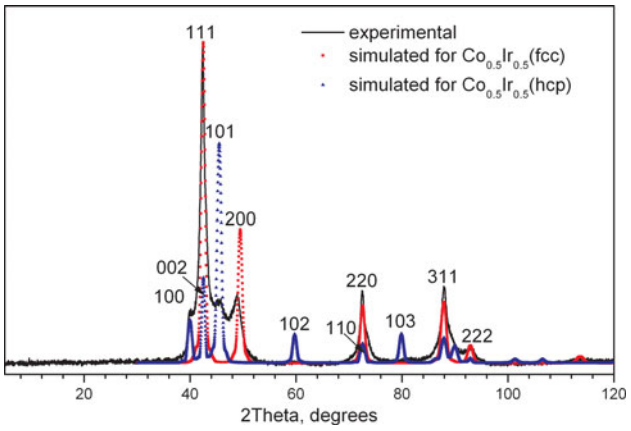

Figure 1. (Color online) Experimental XRD pattern (solid curve) and simulated ones to fcc (squares) and hcp (triangles) structures with crystallite size about 10 nm.

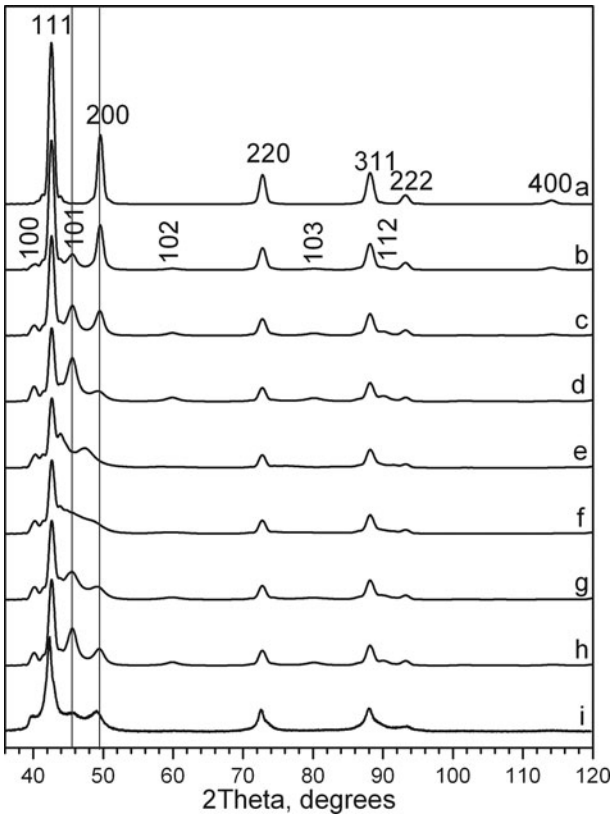

Figure 2. XRD patterns simulated for 10 nm size particles having (a) fcc structure; (b–h) domain structure; average thicknesses of the domains of the fcc and hcp structures: (b) 8.4 and 2.1 nm; (c) 3.2 and 2.1 nm; (d) 1.4 and 2.1 nm; (e) 0.9 and 0.9 nm; (f) 1.1 and 1.1 nm; (g) 1.4 and 1.4 nm; (h) 2.1 and 2.1 nm; (i) experimental XRD pattern.

https://doi.org/10.1017/S0885715617000367 Published online by Cambridge University Press

TABLE I. The peak broadening [full width at half maximum (FWHM)] for the reflections of domain structure.

2θ, grad.	(*hkl*), struct.	FWHM	2θ, grad.	(*hkl*), struct.	FWHM
40.11	(*100*), hcp	1.20	72.56	(*110*), hcp + (*220*), fcc	1.28
42.38	(*002*), hcp + (*111*), fcc	1.14	81.05	(*103*), hcp	1.29
45.47	(*101*), hcp	4.34	87.98	(*200*), hcp + (*311*), fcc	1.62
48.91	(*200*), fcc	1.95	91.91	(*112*), hcp	n/o
60.00	(*102*), hcp	n/o	91.65	(*222*), fcc	2.20

TABLE II. *R*-factors (%) calculated for different values of W_2 and P_{22} parameters.

$P_{22}\rightarrow$	0.45	0.5	0.55	0.60	0.65	0.70
$\langle L_{hcp}\rangle$, nm$\rightarrow$	0.8	0.9	1.0	1.1	1.2	1.4
$W_2\downarrow$						
0.30	–	7.6	7.9	8.3	–	–
0.35	7.3	6.8	6.7	6.7	7.4	–
0.40	–	7.2	6.6	**6.4**	6.7	7.5
0.45	–	8.1	7.6	7.3	7.2	–

of three-layered fragments of fcc (for example, AB–CA–BC) and hcp (for example, AB–AB–AB) structures respectively. $W_{111} = W_1 \bullet P_{11} \bullet P_{11}$ and $W_{222} = W_2 \bullet P_{22} \bullet P_{22}$ are the probabilities of appearance of four-layered fragments of fcc and hcp structures respectively and so on. Therefore, parameters P_{11} and P_{22} determine the average thicknesses of fcc and hcp domains, respectively. Parameters W_1 and W_2 define the ratio of the average thickness of the domains having fcc structure to the average thickness of the domains having hcp structure ($W_1/W_2 = (1 - W_2)/W_2$). It is enough to define only two parameters: W_1 and P_{11} or W_2 and P_{22}. As it was mentioned earlier we varied W_2 and P_{22}.

It is interesting to analyze how inclusions of hcp domains into fcc matrix influence on the diffraction patterns. First, we fixed the parameter $P_{22} = 0.8$ and let the parameter W_2 sequentially increases up to 0.2, 0.4, and 0.6. These values of parameters correspond to the average thickness of the domains having hcp structure equal to 2.1 nm and to the ratio of the average thickness of the domains of the fcc structure to the average thickness of the domains of the hcp structure: 0.8/0.2, 0.6/0.4, and 0.4/0.6. Thereby the average thickness of the domains of the fcc structure was 8.4 nm [Figure 2(b)], 3.2 nm [Figure 2(c)], and 1.4 nm [Figure 2(d)], respectively. One can see that inclusion of hcp lamellar domains into fcc structure leads to the appearance of peaks additional with respect to the peaks of the fcc structure [marked on Figure 2(a)]. These superstructural peaks arise at the positions of the peaks characteristic of the hcp structure [marked on Figure 2(b)] or near them. The higher is the value of W_2, the more intensive are the additional peaks of diffuse scattering. The width of the *111, 220*, and *311* peaks hardly changes. The intensity of the *111* peak gradually decreases, the *200* peak gradually shifts toward lower angles and broadens with W_2 increase.

Then, we fixed the parameter $W_2 = 0.5$ and varied the parameter P_{22} (0.5, 0.6, 0.7, and 0.8). These values correspond to the same average thickness of the two types of domains, which are equal to 0.9 nm [Figure 2(e)], 1.1 nm [Figure 2(f)], 1.4 nm [Figure 2(g)], and 2.1 nm [Figure 2(h)], respectively. Figures show that very small average thicknesses of domains (0.9 nm) produce peaks of diffuse scattering shifted toward smaller angles relative to the positions of the *200* (fcc) and *101* (hcp) peaks. When the average thicknesses of

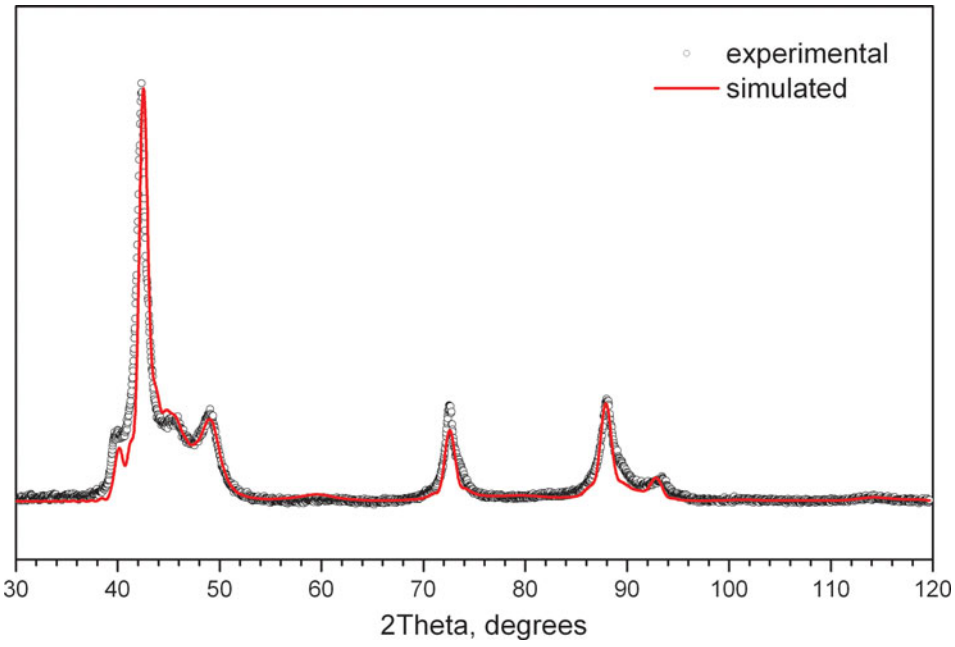

Figure 3. (Color online) Experimental (dotted curve) and simulated (solid curve) XRD patterns (average crystallite size $10 \times 10 \times 10$ nm^3, $R = 6.4\%$).

https://doi.org/10.1017/S0885715617000367 Published online by Cambridge University Press

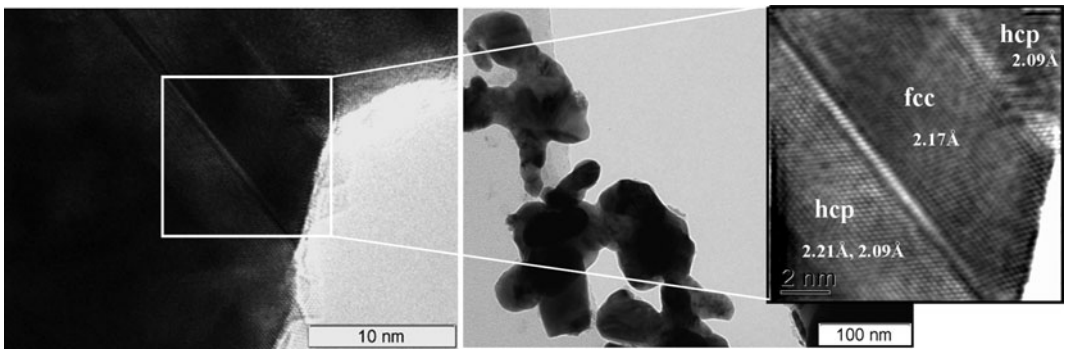

Figure 4. TEM photographs of nanoparticles CoIr with the domain structure.

fcc and hcp domains are about 1.1 nm, one broad peak of diffuse scattering is observed in the angle range 43°–52°. Increase in the average thickness of domains (1.4 and 2.1 nm) leads to the appearance of the diffuse peaks in the positions of the *200* (fcc) and *101* (hcp) peaks.

To fit the experimental XRD data [Figure 2(i)] the parameters W_2 and P_{22} were varied with step of 0.05 and corresponding XRD patterns were simulated. Calculated *R*-factors are listed in Table II. The best fit was obtained for a model in which particles have about 10 nm size, average thicknesses of lamellar domains having fcc and hcp structures are 1.7 and 1.1 nm, respectively (Figure 3).

For confirmation of the XRD results samples were investigated by the TEM. Figure 4 shows that particles of Co–Ir alloy consist of two type lamellar domains having fcc and hcp structures. The ratio of Co:Ir measured by the EDXA is 50:50 at.% with deviation up to 1 at.% obtained at the different locations of sample.

Authors think that it is necessary to make an additional *in situ* XRD experiment to confirm that this domain structure is formed in the thermolysis process at and not during cooling.

IV. CONCLUSION

The XRD pattern of nanosized equimolar solid solution CoIr prepared by thermolysis of $[Co(NH_3)_6][Ir(C_2O_4)_3]$ contains peaks characteristic of both fcc and hcp structures. Moreover, *101* peak of hcp modification is substantially wider than *100* and *002* peaks, *102* and *103* are very broad and almost invisible. Peak *200* of fcc structure is wider than the other peaks of this modification and slightly shifted toward lower angles. It was shown by the simulation of XRD patterns that particles of the CoIr alloy are nanoheterogeneous and consist of lamellar domains having fcc and hcp structures. The best fit was obtained for the following model parameters: an average crystallites size is about 10 nm, average thicknesses of the fcc and hcp domains are 1.7 and 1.1, respectively. The presence of domain structure was confirmed by TEM data.

ACKNOWLEDGEMENT

This work was supported by the Russian Foundation for Basic Research (Grant no. 14-03-00129-a).

Asanova, T., Asanov, I., Zadesenets, A., Filatov, E., Plyusnin, P., Gerasimov, E., and Korenev, S. (**2016**). "Study on thermal decomposition of double complex salt $[Pd(NH_3)_4][PtCl_6]$," J. Therm. Anal. Calorim. **123**(2), 1183–1195.

Cherepanova, S. V. (**2012**). "X-ray scattering on one-dimensional disordered structures," J. Struct. Chem. **53**, 109–132.

Cherepanova, S. V. and Tsybulya, S. V. (**2004**). "Simulation of X-ray powder diffraction patterns for one-dimensionally disordered crystals," Mater. Sci. Forum **443–444**, 87–90.

Filatov, E. Yu., Yusenko, K. V., Vikulova, E. S., Plyusnin, P. E., and Shubin, Yu. V. (**2009**). "XRD investigation and thermal properties of $[Ir(NH_3)_6][Co(C_2O_4)_3]\cdot H_2O$ and $[Co(NH_3)_6][Ir(C_2O_4)_3]$ precursors for $Co_{0.50}Ir_{0.50}$," Z. Kristallogr. Suppl. **30**, 263–268.

Firdous, N., Janjua, N. K., Qazi, I., and Wattoo, M. H. S. (**2015**). "Optimal Co-Ir bimetallic catalysts supported on gamma-Al_2O_3 for hydrogen generation from hydrous hydrazine," Int. J. Hydrog. Energy (In press). doi: 10.1016/j.ijhydene.2015.10.084.

Köster, W. and Horn, E. (**1952**). "Zustandsbild Und Gitterkonstanten Der Legierungen Des Kobalts Mit Rhenium, Ruthenium, Osmium, Rhodium Und Iridium" (in German)," Z. Metallkd., **43**(12), 444–449.

Kraus, W. and Nolze, G. (**2000**). *PowderCell 2.4, Program for the Representation and Manipulation of Crystal Structures and Calculation of the Resulting X-ray Powder Patterns* (Federal Institute for Materials Research and Testing, Berlin).

Krumm, S. (**1995**). "An interactive windows program for profile fitting and size/strain analysis" Mater. Sci. Forum **228–231**, 183–188.

Liu, Z. and Sadler, P. J. (**2014**). "Organoiridium complexes: anticancer agents and catalysts," Acc. Chem. Res. **47**, 1174–1185.

Martynova, S. A., Filatov, E. Yu., Korenev, S. V., Kuratieva, N. V., Sheludyakova, L. A., Plusnin, P. E., Shubin, Yu. V., Slavinskaya, E. M., and Boronin, A. I. (**2014**). "Low temperature synthesis of Ru–Cu alloy nanoparticles with the compositions in the miscibility gap," J. Solid State Chem. **212**, 42–47.

Plyusnin, P. E., Makotchenko, E. V., Shubin, Y. V., Baidina, I. A., Korolkov, I. V., Sheludyakova, L. A., and Korenev, S. V. (**2015**). "Synthesis, crystal structures, and characterization of double complex salts $[Au(en)_2][Rh(NO_2)_6]\cdot 2H_2O$ and $[Au(en)_2][Rh(NO_2)_6]$," J. Mol. Struct. **1100**, 174–179.

Potemkin, D. I., Filatov, E. Yu., Zadesenets, A. V., Snytnikov, P. V., Shubin, Yu. V., and Sobyanin, V. A. (**2012**). "Preferential CO oxidation over bimetallic Pt–Co catalysts prepared via double complex salt decomposition," Chem. Eng. J. **207–208**, 683–689.

Potemkin, D. I., Semitut, E. Y., Shubin, Y. V., Plyusnin, P. E., Snytnikov, P. V., Makotchenko, E. V., Osadchii, D. Y., Svintsitskiy, D. A., Venyaminov, S. A., Korenev, S. V., and Sobyanin, V. A. (**2014**). "Silica, alumina and ceria supported Au-Cu nanoparticles prepared via the decomposition of $[Au(en)_2]_2[Cu(C_2O_4)_2]_3\cdot 8H_2O$ single-source precursor: synthesis, characterization and catalytic performance in CO PROX," Catal. Today **235**, 103–111.

Slavcheva, E., Borisov, G., Lefterova, E., Petkucheva, E., and Boshnakova, I. (**2015**). "Ebonex supported iridium as anode catalyst for PEM water electrolysis," Int. J. Hydrog. Energy **40**, 11356–11361.

Tetlow, H., de Boer, J. P., Ford, I. J., Vvedensky, D. D., Curcio, D., Omiciuolo, L., Lizzit, S., Baraldi, A., and Kantorovich, L. (**2016**). "Ethylene decomposition on Ir(111): initial path to graphene formation," Phys. Chem. Chem. Phys. **18**, 27897–27909.

Tsybulya, S. V., Cherepanova, S. V., Khasin, A. A., Zaikovskii, V. V., and Parmon, V. N. (**1999**). "Structure of heterogeneous coherent states in fine grains of metallic cobalt," Dokl. Phys. Chem. **366**(1–3), 143–146.

Vedyagin, A. A., Volodin, A. M., Stoyanovskii, V. O., Kenzhin, R. M., Slavinskaya, E. M., Mishakov, I. V., Plyusnin, P. E., and Shubin, Y. V. (**2014**). "Stabilization of active sites in alloyed Pd–Rh catalysts on γ-Al_2O_3 support," Catal. Today **238**, 80–86.

Zhong, H.-J., Lu, L., Leung, K.-H., Wong, C. C. L., Peng, C., Yan, S.-C., Ma, D.-L., Cai, Z., Wand, H.-M. D., and Leung, C.-H. (**2015**). "An iridium (III)-based irreversible protein–protein interaction inhibitor of BRD4 as a potent anticancer agent," Chem. Sci. **6**, 5400–5408.

https://doi.org/10.1017/S0885715617000367 Published online by Cambridge University Press